LETTERS
PUBLISHED ONLINE: 25 NOVEMBER 2012 | DOI: 10.1038/NMAT3492
nature materials

Glycans pattern the phase behaviour of lipid membranes

Anand Bala Subramaniam[1]*†, Guido Guidotti[2], Vinothan N. Manoharan[1] and Howard A. Stone[3]*

Hydrated networks of glycans (polysaccharides)—in the form of cell walls, periplasms or gel-like matrices—are ubiquitously present adjacent to cellular plasma membranes[1–4]. Yet, despite their abundance, the function of glycans in the extracellular milieu is largely unknown[5]. Here we show that the spatial configuration of glycans controls the phase behaviour of multiphase model lipid membranes: inhomogeneous glycan networks stabilize large lipid domains at the characteristic length scale of the network, whereas homogeneous networks suppress macroscopic lipid phase separation. We also find that glycan-patterned phase separation is thermally reversible—thus indicating that the effect is thermodynamic rather than kinetic—and that phase patterning probably results from a preferential interaction of glycans with ordered lipid phases. These findings have implications for membrane-mediated transport processes[6–8], potentially rationalize long-standing observations that differentiate the behaviour of native and model membranes[9–13] and may indicate an intimate coupling between cellular lipidomes and glycomes.

Glycan-rich cell walls or extracellular matrices that are rigid in comparison with the plasma membrane surround most cells[1–4]. However, it is often reported that rigid supports cause non-equilibrium[14–16] behaviour of lipids and proteins in model lipid membranes. Indeed, although there are many reports of lipid membranes supported on non-biological polymers such as polyethylene glycol, polyacrylamide or polyethyleneimine[17–20] that seek to mitigate non-equilibrium behaviour, such systems have been used mainly to study the effects of polymer hydration[21] on the mobility of lipids[18,19], or to preserve the function of transmembrane protein inclusions[17,22]. Furthermore, although it is widely acknowledged that a greater understanding of parameters that influence the size and length scale of membrane domains is required[6–13,23,24], as far as we know systematic studies exploring the effects of biopolymers (the subject of this Letter) or other more commonly used polymers in the field[17–20] on the phase behaviour of lipid membranes have not been conducted. To investigate the possible effects of biologically relevant polymers—specifically glycans—on the behaviour of membranes, we designed an *in vitro* solid-supported experimental platform that allows, through fluorescent labelling and confocal microscopy, the study of lipid membranes interacting with hydrated networks of glycans with an arbitrary glycan composition and variable network configurations.

We prepare glycan networks on flat hydrophilic surfaces using instability-driven pattern formation (see Methods and Supplementary Information for further details). Spontaneous rupture of giant lipid vesicles provided two-dimensional (2D) lipid membrane patches that interact with the glycan networks. Lipid membranes were labelled with trace amounts of fluorescent probes to visualize phase behaviour. Vesicle rupture was performed at 65 °C to ensure that the membranes, which consisted of up to five distinct lipid species, were fully mixed in a single macroscopically uniform liquid phase[11,13]. The glycan network–lipid membrane system was then cooled to room temperature for subsequent experiments. Whereas the lateral configuration of the glycan network does not change with temperature (Supplementary Fig. S10), as we outline below, the lipid membrane is free to undergo temperature-induced phase transitions. Although the images shown in this report are of fluorescein isothiocyanate (FITC)-labelled glucomannan, we find that all of the glycans tested have the same effects on our membranes, and thus we refer generically to glycans in the remainder of this report.

We prepare two classes of glycan networks: inhomogeneous glycan networks, characterized by the presence of distinct glycan-rich and glycan-poor domains (Fig. 1a–d), and homogeneous glycan networks, characterized by a uniform distribution of glycans with any inhomogeneities below the resolution limit of the microscope (∼300 nm; Fig. 1e). To obtain a quantitative description of the network structure, we calculate the power spectral density (PSD) of the florescence intensity. For inhomogeneous networks, pronounced peaks (red arrows), typically one but sometimes two, can be discerned in the PSD curve at characteristic wavenumbers (Fig. 1f–i). We term the reciprocal of these wavenumbers as the characteristic length scale of the network, $L_{network}$. For homogeneous networks, as expected, no pronounced peaks are present in the PSD curve, which confirms the lack of resolvable structures (Fig. 1j).

We find that multiphase membranes that rest on inhomogeneous glycan networks exhibit macroscopic time-stable lipid domains at room temperature (Fig. 2 a,b). Membranes in a single phase, on the other hand, are insensitive to the glycan network (Supplementary Fig. S1). Liquid-ordered (L_o) and solid-ordered (S_o) domains coexisting with liquid-disordered (L_d) domains on the glycan networks appear identical in shape, although other physical properties such as lipid diffusion coefficients vary as expected on the basis of the known physical properties of these phases (Supplementary Information and Figs S4 and S5). The lipid domains as a whole do not exhibit Brownian motion, have non-fluctuating boundaries and do not coarsen over a two-day period, which differentiates their dynamics from multiphase lipid vesicles[11,25] and from solid-supported double bilayers[15,26,27]. Fourier analysis of the fluorescence intensity of the lipid-phase-sensitive probes allows us to determine the characteristic length scale of the phase-separated domains, L_{lipid}: we find that L_{lipid} (green arrows) matches $L_{network}$ (red arrows; Fig. 2c,d). Indeed, L_{lipid} is almost perfectly correlated with $L_{network}$ in multiphase membranes resting on inhomogeneous

[1]School of Engineering and Applied Sciences, Harvard University, Cambridge, Massachusetts 02138, USA, [2]Department of Molecular and Cellular Biology, Harvard University, Cambridge, Massachusetts 02138, USA, [3]Department of Mechanical and Aerospace Engineering, Princeton University, Princeton, New Jersey 08544, USA. †Present address: Department of Chemistry and Chemical Biology, Harvard University, Cambridge, Massachusetts 02138, USA.
*e-mail: balasubr@fas.harvard.edu; hastone@princeton.edu.

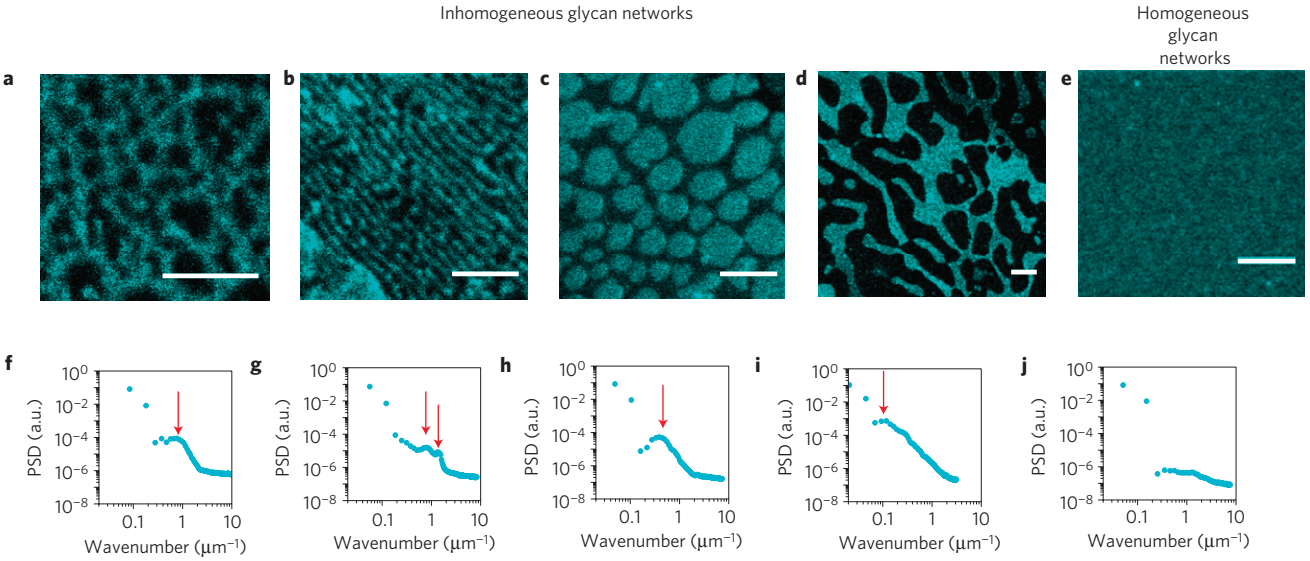

Figure 1 | Preparation of hydrated glycan networks with varying spatial configurations. a–d, Inhomogeneous glycan networks are characterized by the presence of optically resolvable glycan-rich and glycan-poor domains. The shape and interdomain spacing vary with the preparation conditions. **e**, Homogeneous glycan networks appear uniform with no resolvable glycan domains. **f–i**, The PSD of the networks in **a–d** reveals a pronounced peak (red arrow), at a wavenumber, sometimes two, signifying the dominant length scale(s) present in the image. We call the reciprocal of these wavenumbers the characteristic length scale(s) of the network, $L_{network}$. For the sample networks shown here, $L_{network} = 1.31\,\mu m$ (**f**); first peak, 1.31 μm, second peak, 0.74 μm (**g**); 2.58 μm (**h**), 8.50 μm (**i**). **j**, For the homogeneous glycan network in **e**, there are no pronounced peaks in the PSD, signifying the absence of a dominant length scale, at least down to optical resolution (~300 nm in our set-up). Note also the distinct difference in the shape of the PSD curves of inhomogeneous (**f–i**) and homogeneous networks (**j**). Scale bars, 5 μm.

glycan networks (linear correlation coefficient 0.9975, $n = 15$ for both L_o/L_d and S_o/L_d phases; Fig. 2e). Thus, we conclude that the glycans in the network set the characteristic length scale of phase separation of the adjacent multiphase membrane, L_{lipid}.

How do the glycans set L_{lipid}? We use two methods to analyse the positions of lipid domains with respect to the glycan network. First, we compare the greyscale intensity of L_d and L_o pixels against the greyscale intensity of glycan pixels and plot the resulting data sets as colour-coded contour plots. For L_o-sensitive probes, a high density of points lies along the diagonal, which demonstrates the co-localization of L_o-preferring probes and glycans (Fig. 2f). In contrast, for L_d-sensitive probes, a high density of points along the two axes and away from the diagonal indicates anti-correlation of L_d-preferring probes and glycans (Fig. 2g, also see Supplementary Fig. S9 for multi-image analysis).

Second, we cross-correlate glycan images with L_d and L_o images and calculate the radial average of the resulting 2D cross-correlation matrices for $n = 15$ L_o/L_d bilayers. We show the cross-correlation curves corresponding to the images in Fig. 2a as Fig. 2h. We find that L_o/glycan cross-correlation curves show a large positive peak at zero lag (amplitude = 0.72 for the curve in Fig. 2h, 0.63 ± 0.09 for $n = 15$ L_o/glycan images), which indicates that the locations of L_o domains are positively correlated with those of glycan-rich domains. On the other hand, L_d/glycan cross-correlation curves show a large negative peak at zero lag (amplitude = −0.83 for the curve in Fig. 2h, -0.72 ± 0.09 for $n = 15$ L_d/glycan images), which indicates that the position of L_d domains is negatively correlated with the position of glycan-rich domains. The cross-correlation length ~1 μm (blue arrows) is in good agreement with $L_{network}$ found from the PSD in Fig. 2c. Similar analyses performed on $S_o - L_d$ membranes indicate that S_o domains co-localize with glycan-rich regions (Fig. 2i–k; mean peak amplitude $= 0.61 \pm 0.17$ for $n = 15$ S_o/glycan images, $= -0.77 \pm 0.13$ for $n = 15$ L_d/glycan images). We thus conclude that the more ordered L_o and S_o phases of multiphase membranes have an affinity for glycan-rich regions. This affinity dictates the patterning of the characteristic length scale of the lipids, L_{lipid}, at the characteristic length scale of the network, $L_{network}$.

The irregular shape of L_o and L_d domains is noteworthy because these phases in the absence of glycans are strongly influenced by line tension and thus minimize boundary perimeters by forming a small number of large circular domains[12]. In our sample of 15 L_o/L_d membranes, these present excess perimeter boundaries ranging from 600 to 1,200% of the theoretical minimum extrapolated from the domain areas. One possible explanation for the excess boundaries is kinetic trapping[14]. If this were the case, we would expect the membranes to not undergo reversible temperature-induced phase transitions[11,13,14,28]. We test for kinetic trapping by subjecting the membranes to thermal cycles. We find that lipid membranes on inhomogeneous glycan networks clearly maintain thermodynamic transitions: domains melt above the membrane transition temperature and reappear below the transition temperature (Fig. 3). L_{lipid}, however, remains the same after the thermal cycle (Fig. 3). We conclude that the lipid domains are not trapped and that we are observing the inhomogeneous glycan network strongly modifying the characteristic length scale of phase separation, L_{lipid}. Although the phase behaviour of membranes with kinetically trapped domains is subject to several subtleties such as the incomplete dissolution of domains when temperature is cycled[26], it is important to note, however, that unlike in previous reports[11,13,14,26,28], we ensured that our vesicles were in a single uniform phase on initial fusion onto the glycan networks.

How do multiphase membranes behave on homogeneous glycan networks, where there is no discernible $L_{network}$? We find that multiphase membranes that rest on homogeneous glycan networks appear uniform (Fig. 4a,b). Fourier analysis confirms that there is no characteristic length scale of phase separation, L_{lipid} (Fig. 4c,d). Furthermore, intensity contour plots show a clustering of points in intensity phase space of L_o, S_o and L_d-sensitive probes (Fig. 4e,f,h,i), and cross-correlation curves are flat (Fig. 4g,j). Indeed, peak amplitudes at zero lag for these membranes are an order of magnitude smaller in comparison with those

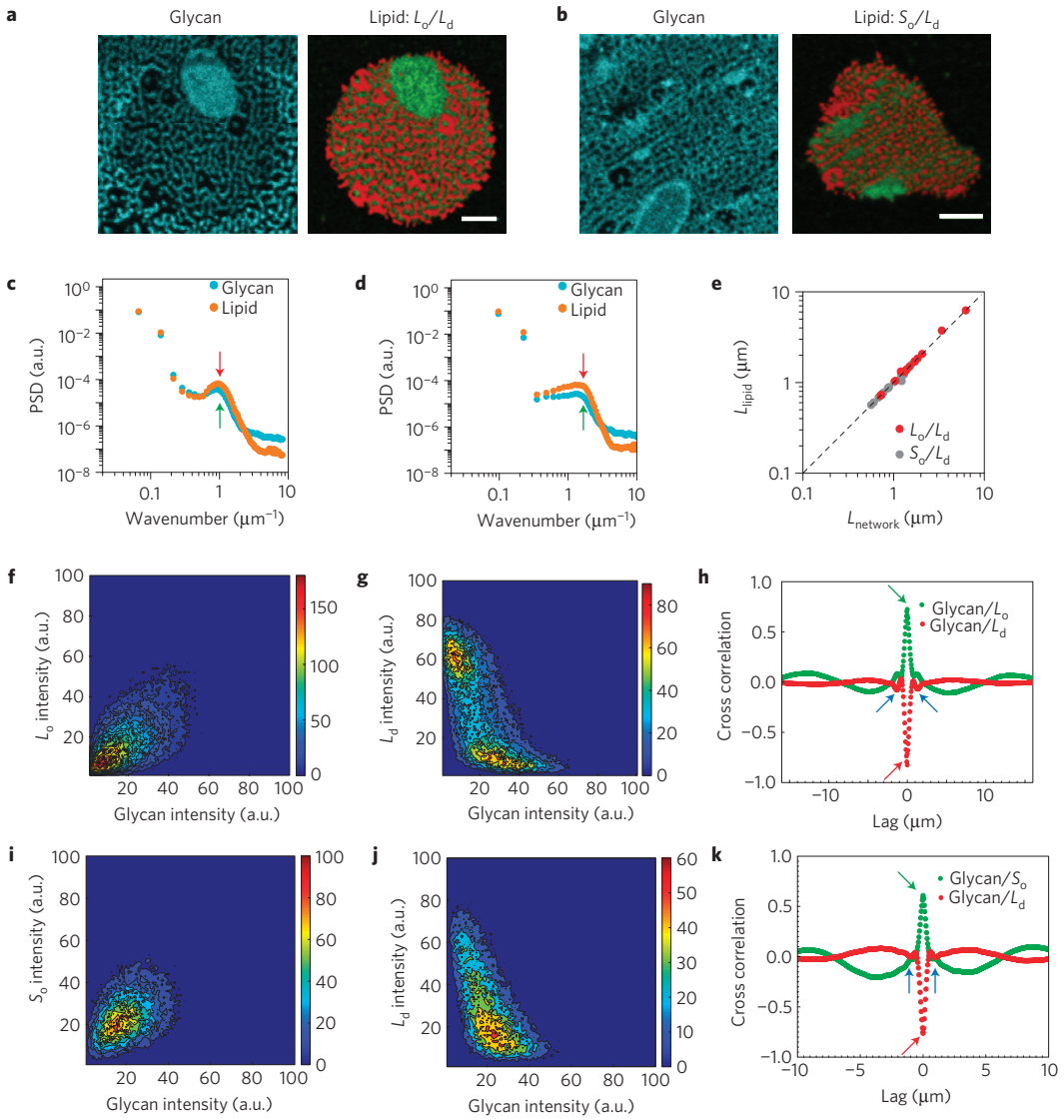

Figure 2 | Inhomogeneous glycan networks pattern the formation of macroscopic time-stable lipid domains in multiphase membranes. **a**,**b**, Inhomogeneous glycan networks pattern the formation of phase-separated lipid domains in multiphase membranes showing L_o/L_d (**a**) and S_o/L_d coexistence (**b**). **c**,**d**, PSDs show clearly that L_{lipid} (red arrows) matches $L_{network}$ (green arrows). **e**, Plot of $L_{network}$ versus L_{lipid}, identified from the PSD of $n = 15$ membranes in the L_o/L_d phases and $n = 15$ membranes in the S_o/L_d phases. The diagonal line is a guide to the eye showing the case for perfect correlation. There is strong correlation between $L_{network}$ and L_{lipid}; linear correlation coefficient, $r = 0.9975$. **f**, Contour plot of the greyscale intensity of L_o-preferring probes versus glycans showing a high density of points along the diagonal, indicative of co-localization of L_o domains and glycans. **g**, For L_d-sensitive probes, a high density of points along the two axes and away from the diagonal indicates anti-correlation of L_d domains and glycans. **h**, Radial average of the normalized cross-correlation matrix of the glycan network and L_o domains (green filled circles), and the glycan network and L_d domains (red filled circles). The large positive peak at zero lag (green arrow) shows that L_o domains are positively correlated with the glycans in the network, whereas the large negative peak at zero lag (red arrow) shows that L_d domains have a negative correlation with the distribution of glycans in the network. Secondary peaks (blue arrows) show the cross-correlation lengths. **i**–**k**, Similar analysis performed on the S_o/L_d membrane shown in **b** shows that S_o domains also rest on glycan-rich regions. Note that the close proximity of the membrane to the glycan layer results in the quenching of fluorescence intensity of the glycans due to fluorescence resonance energy transfer between rhodamine in the L_d probes and FITC in the glycans (see Supplementary Information for further details). Scale bars, 5 μm.

on inhomogeneous glycan networks (values $= -0.05 \pm 0.09$ and 0.07 ± 0.14 for $n = 15$ L_o/glycan and L_d/glycan images, respectively, and $= -0.01 \pm 0.03$ and -0.02 ± 0.10 for $n = 15$ S_o/glycan and L_d/glycan images, respectively). These results are consistent with the conclusion that there is no macroscopic phase separation of the lipids in the membranes, and contrasts sharply with the behaviour of lipids in similar membranes on inhomogeneous glycan networks (Fig. 2a,b) and in giant vesicles (Supplementary Fig. S2d,e). We can neither support nor exclude the possibility that nanoscale domains or short-lived rafts with length scales below the resolution limit of the microscope[29] may be present in multiphase membranes on homogeneous glycan networks.

Differences in roughness[24] might be a starting point for a mechanistic explanation of the effects of glycans on lipid membranes. We image our glycan networks and bare oxidized poly(dimethyl)siloxane (PDMS) with an atomic force microscope (AFM). Typical images of the inhomogeneous and homogeneous networks are shown in Fig. 5a,b. AFM phase imaging indicates that the number of glycan molecules per unit area is lower in the glycan-poor regions than in the glycan-rich regions (Fig. 5c,

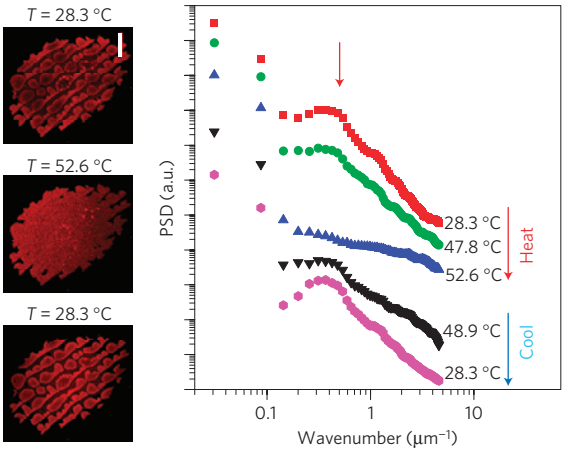

Figure 3 | Lipid domains on inhomogeneous glycan networks are in thermal equilibrium as evidenced by reversible temperature-induced phase transitions. When heated, lipid domains melt, and the fluorescent-phase-sensitive probes distribute uniformly in the lipid membrane. When the membrane is cooled the domains reappear. The peak in the PSD curve (red arrow) confirms that L_{lipid} is preserved at the end of the thermal cycle. The PSD curves have been offset for clarity and the membrane is resting on an unlabelled hyaluronic acid network. The duration of the cycle is 10 min. Scale bar, 15 μm.

also see Supplementary Section S6). We calculate the root mean square roughness ($R_{r.m.s.}$) values over a 1 × 1 μm square region to allow comparison of the roughness values between inhomogeneous glycan networks (we placed the sampling box over glycan-rich domains and glycan-poor domains of sufficient size to fully enclose the 1 × 1 μm box). For homogeneous networks where there are no domains and for bare PDMS, the sampling box was placed at random. We found that the $R_{r.m.s.}$ values between the glycan-rich and glycan-poor regions were similar within experimental error (Fig. 5d). The $R_{r.m.s.}$ values of the homogeneous glycan networks were also indistinguishable within experimental error, whereas bare oxidized PDMS had a lower $R_{r.m.s.}$ (Fig. 5e).

The glycan-rich regions are raised with respect to the glycan-poor regions (Fig. 5a). Naively, gross changes in topography might be an alternative explanation for our observation of phase patterning in multiphase membranes. How do we untangle putative gross topographical effects from other chemical or microstructural features of the glycan network? We devised a method to test for the effects of topography by making replicas[27] of the glycan network in PDMS. These replicas preserve the gross topography of the network while being composed purely of inert PDMS.

We deposit multiphase membranes on the PDMS replicas and visualize them with the confocal microscope (Fig. 5f,g). We use confocal reflection microscopy to visualize the replica, because it is not fluorescent; the greyscale intensity of the images of the replica corresponds to the height and curvature of the surface, and not the

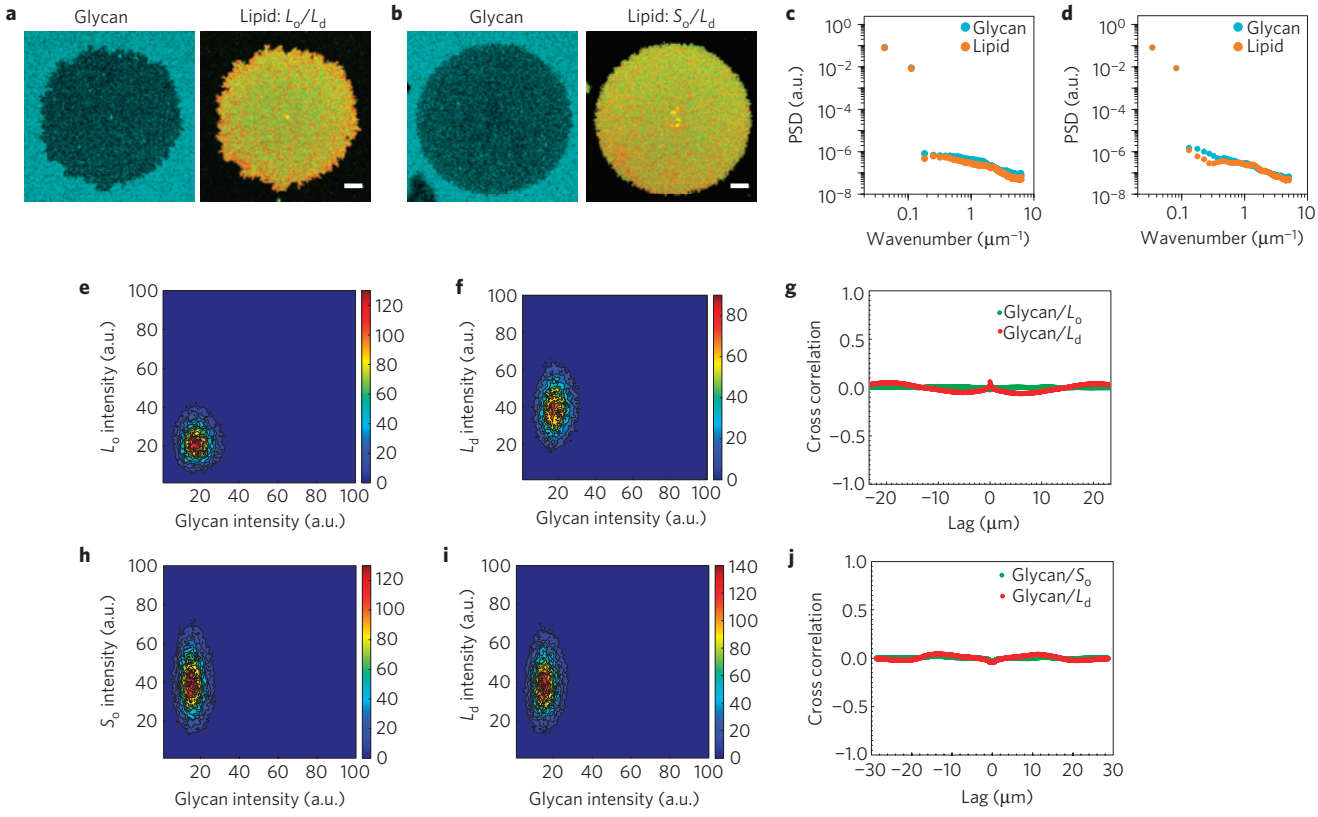

Figure 4 | Homogeneous glycan networks suppress macroscopic phase separation in multiphase lipid membranes. a,**b**, Multiphase membranes on homogeneous glycan networks appear uniform. **c**,**d**, PSD curves confirm the lack of a characteristic length scale in the membrane (orange circles). Glycan PSDs are shown as cyan circles. **e**,**f**, Contour plots of the greyscale intensity of L_o-preferring probes versus glycans and L_d-sensitive probes versus glycans show a cluster of points in intensity phase space. **g**, Radial averages of the normalized cross-correlation matrices of the glycan network and L_o image (green filled circles), and the glycan network and L_d image (red filled circles). No clear correlations are evident. **h**–**j**, Analysis performed on the S_o/L_d membrane shown in **b** gives a similar result. The results of both methods of analysis are consistent with the conclusion that there is no macroscopic phase separation of multiphase lipid membranes on homogeneous networks. Note that the close proximity of the membrane to the glycan layer results in the quenching of fluorescence intensity of the glycans due to fluorescence resonance energy transfer between rhodamine in the L_d probes and FITC in the glycans (see Supplementary Information for further details). Scale bars, 5 μm.

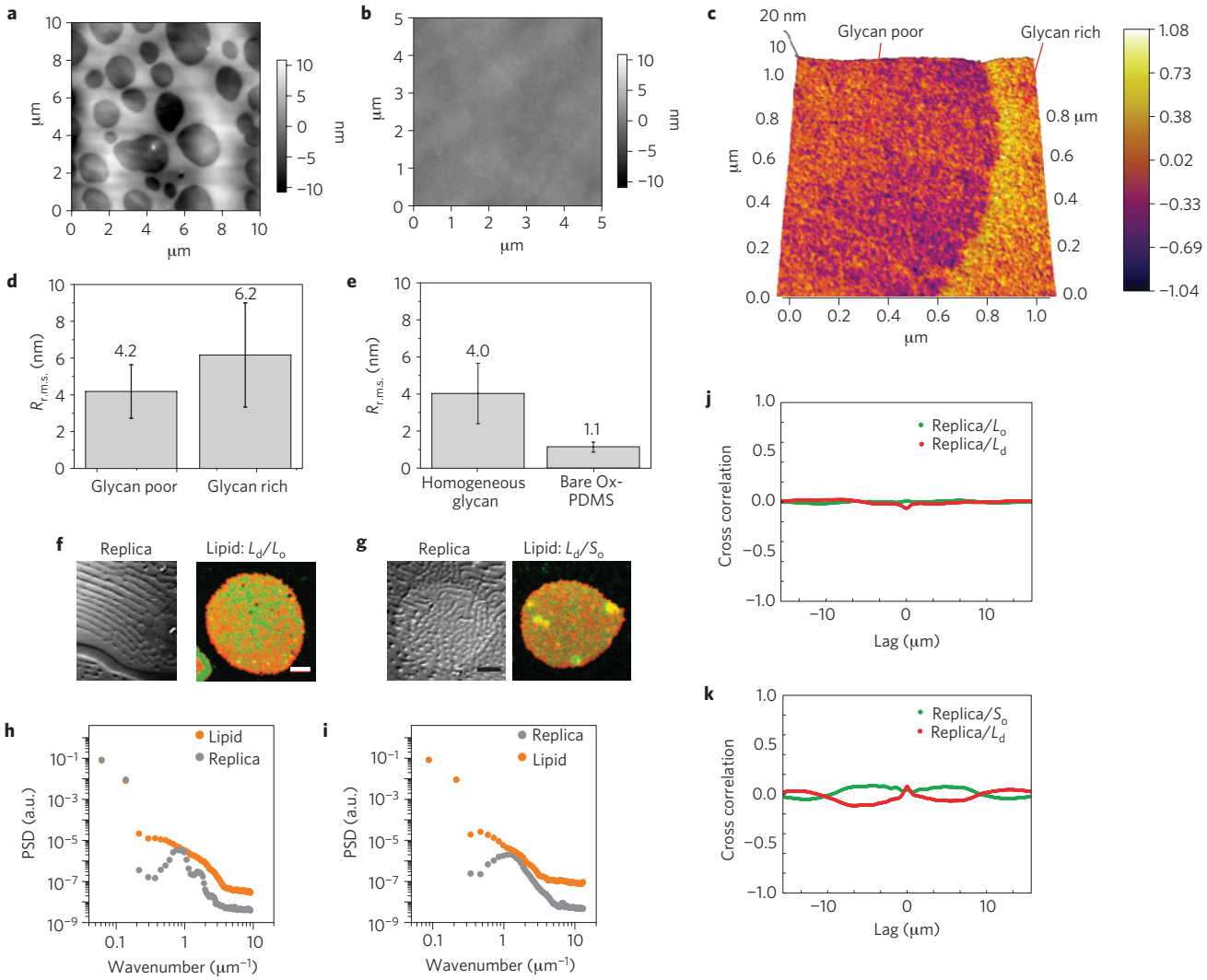

Figure 5 | Gross topography and microstructural roughness of the inhomogeneous glycan networks are not the dominant mechanism for the patterning of phase separation of lipid membranes. a,**b**, AFM images of typical inhomogeneous and homogeneous glycan networks. The dark grey regions are glycan-poor domains and the light grey regions are glycan-rich domains. **c**, A 3D reconstruction of the inhomogeneous glycan network overlaid with AFM phase information. The phase image was false coloured according to phase angle, with glycans appearing yellow whereas the substrate appears purple. It is clear that glycans are present at a lower density in the glycan-poor regions. **d**, $R_{r.m.s.}$ values indicate no significant difference in roughness between the glycan-rich and glycan-poor regions. **e**, $R_{r.m.s.}$ values of homogeneous networks were comparable to those measured on inhomogeneous networks. Bare ox-PDMS (that is, substrate devoid of glycans) was significantly smoother. Error bars are standard deviations for $n = 10$. **f**,**g**, Multiphase membranes deposited on the PDMS replicas under similar conditions as those for the membranes shown in Figs 2 and 4. The replica surface, which is not fluorescent, was imaged through confocal reflection microscopy (glycans cannot be imaged through reflection, probably because the highly hydrated layers lack optical contrast with the surrounding water). Bright yellow circles on the membrane are lipid vesicles adhering to the bilayer patch. Scale bars, 5 μm. **h**,**i**, PSDs of the bilayer (filled orange circles) show that the lipids do not respond to the dominant length scale of the PDMS replica (filled grey circles). **j**,**k**, Radial averages of the normalized cross-correlation matrices of the replica and L_o/S_o images (green filled circles), and the replica and L_d images (red filled circles). No clear correlations are evident.

number density of glycans on the surface (which is what is measured in the fluorescence images). We perform Fourier analysis, similar to the ones performed for the glycan networks, on these images. It is clear from the images, the PSDs and the cross-correlation analysis that the replicas do not pattern the phase separation of the membranes (Fig. 5h–k). It might be possible that there are differences at the nanoscale regarding the contours of the lipid bilayers and the substrates, but it is unlikely to be a main factor given the many reports that lipid bilayers follow faithfully the topography of even highly rough silica substrates[15,24] (Supplementary Section S7).

Our experimental results are reproducible for all of the glycans tested (hyaluronic acid, heparan sulphate, pectin, inulin, carboxymethyl cellulose, glucomannan, dextran and Ficoll), various lipid species within the coexistence regimes (such as 1,2-dipalmitoyl-*sn*-glycero-3-phosphocholine (DPPC), brain sphingomyelin (BSM), 1-palmitoyl-2-oleoyl-*sn*-glycero-3-phosphocholine (POPC) and ergosterol) and various fluorescent-probe molecules. Furthermore, extensive control experiments were performed to explore potential fluorescent probe-related artefacts (Supplementary Section S4).

The effect of glycans that we report here could rationalize the discrepancy between previous observations of model lipid membranes, which were without glycans, and the various observations of domains, or lack thereof, in plasma membranes. The plasma membranes of mammalian cells for which nanodomains have been inferred[6,9] are surrounded by gel-like extracellular matrices[1] or

glycan coatings[2]. The absence of macroscopic phase separation of these membranes matches the behaviour of lipid membranes adjacent to homogeneous glycan networks. The lipid domains on inhomogeneous glycan networks, on the other hand, resemble the large stable rafts observed in yeast plasma membranes[30,31] that are adjacent to a multilayered cell wall. We propose that glycans could pattern the phase separation of membranes either by stabilizing ordered lipid phases or by reducing the line tension between coexisting lipid phases. Higher resolution techniques that probe length scales smaller than the optical wavelength[23,32] will be essential for testing this proposal.

Methods

Chemicals. DOPC (1,2-dioleoyl-sn-glycero-3-phosphocholine), DPPC, sphingomyelin (egg), cholesterol (ovine wool), GM1 ganglioside (brain, ovine–ammonium salt) and 1,2-dioleoyl-sn-glycero-3-phosphoethanolamine-*N*-(lissamine rhodamine-B sulphonyl) (ammonium salt) (Rh-DPPE) were purchased from Avanti Polar Lipids. Cholera toxin subunit B (CTXB) conjugated with Alexa647 (A647–CTXB) was purchased from Invitrogen. FITC–glucomannan was purchased from Carbomer. Hyaluronic acid (from rooster comb) was purchased from Sigma Aldrich.

Lipid compositions. Figures 2 and 4: sphingomyelin (egg)/DOPC/cholesterol/Rh-DPPE/GM1 54.8:25:20:0.1:0.1 mol %; Fig. 3 DPPC/DOPC/ergosterol/Rh-DPPE/GM1 54.8:25:20:0.1:0.1 mol%.

Preparation of glycan networks and lipid bilayer patches. Dilute (2 µl, 100 µg ml^{-1}) solutions of glycan dispersed in ultrapure water were deposited on disc-shaped (typically 7.5 mm in diameter) plasma-oxidized PDMS and allowed to dry on a hotplate set at 65 °C. Once the liquid had dried completely, an aqueous buffer (typically 10 mM Tris, 150 mM NaCl and 2 mM $CaCl_2$, at pH 7.5) was added to submerge the surface and rehydrate the glycans. Giant unilamellar vesicles (GUVs) were prepared using the electroformation technique similar to ref. 27. After a 10 min incubation interval, 10 µl of GUV-containing solution (pre-warmed to 65 °C) was added to the chamber above the PDMS disc. GUVs sedimented onto the glycan network, where they ruptured to form 2D supported lipid bilayer patches. After 10 min, the hotplate was turned off and the system was allowed to cool to room temperature. Skimmed milk solution (prepared as a stock solution of 10 mg ml^{-1} in ultrapure water) was added to obtain a final protein concentration of ~0.1 mg ml^{-1} in the chamber and allowed to incubate for at least 10 min to block the regions of the surface not covered by lipid bilayer patches. Then 5 µl A647–CTXB (prepared as a stock solution of 0.1 mg ml^{-1} in phosphate-buffered saline at pH 7.5) was added to the chamber to give a final concentration of ~0.05 mg ml^{-1}. A647–CTXB labels ordered lipid phases.

Imaging. Supported lipid bilayers were imaged with an upright confocal microscope (Zeiss LSM 510) with a ×63/1.0 numerical aperture water dipping objective. FITC was excited with a 488 nm laser with the acquisition acousto-optic tunable filter (AOTF) set at 20%. A band-pass filter 500–510 nm was used in the detection channel. Rhodamine-B was excited with a 543 nm laser with AOTF set at 10%. A band-pass filter 565–615 nm was used in the detection channel. CTXB–A647 was excited with the 633 nm laser, AOTF 30%. A band-pass filter 650–710 nm was used in the detection channel. The images were taken sequentially to further reduce cross-talk between the channels. Images were captured at 14-bits.

Full Methods and any associated references are available in the Supplementary Information.

Received 23 July 2012; accepted 17 October 2012; published online 25 November 2012

References

1. Alberts, B. *et al. Molecular Biology of the Cell* 4th edn (Garland Science, 2002).
2. Laurent, T. & Fraser, J. Hyaluronan. *The FASEB J.* **6,** 2397–2404 (1992).
3. Masako, O. The ultrastructure of yeast: Cell wall structure and formation. *Micron* **29,** 207–233 (1998).
4. Somerville, C. *et al.* Toward a systems approach to understanding plant-cell walls. *Science* **306,** 2206–2211 (2004).
5. Marth, J. D. A unified vision of the building blocks of life. *Nature Cell Biol.* **10,** 1015–1016 (2008).
6. Lingwood, D. & Simons, K. Lipid rafts as a membrane-organizing principle. *Science* **327,** 46–50 (2010).
7. Brown, D. A. & London, E. Functions of lipid rafts in biological membranes. *Annu. Rev. Cell Dev. Biol.* **14,** 111–136 (1998).
8. Engelman, D. M. Membranes are more mosaic than fluid. *Nature* **438,** 578–580 (2005).
9. Munro, S. Lipid rafts: Elusive or illusive? *Cell* **115,** 377–388 (2003).
10. Yethiraj, A. & Weisshaar, J. C. Why are lipid rafts not observed *in vivo*? *Biophys. J.* **93,** 3113–3119 (2007).
11. Veatch, S. L. & Keller, S. L. Organization in lipid membranes containing cholesterol. *Phys. Rev. Lett.* **89,** 268101 (2002).
12. Baumgart, T., Hess, S. T. & Webb, W. W. Imaging coexisting fluid domains in biomembrane models coupling curvature and line tension. *Nature* **425,** 821–824 (2003).
13. McConnell, H. M. & Vrljic, M. Liquid–liquid immiscibility in membranes. *Annu. Rev. Biophys. Biomol. Struct.* **32,** 469–492 (2003).
14. Stottrup, B. L., Veatch, S. L. & Keller, S. L. Nonequilibrium behavior in supported lipid membranes containing cholesterol. *Biophys. J.* **86,** 2942–2950 (2004).
15. Parthasarathy, R., Yu, C. H. & Groves, J. T. Curvature-modulated phase separation in lipid bilayer membranes. *Langmuir* **22,** 5095–5099 (2006).
16. Groves, J. T., Ulman, N. & Boxer, S. G. Micropatterning fluid lipid bilayers on solid supports. *Science* **275,** 651–653 (1997).
17. Tanaka, M. & Sackmann, E. Polymer-supported membranes as models of the cell surface. *Nature* **437,** 656–663 (2005).
18. Smith, H. L. *et al.* Model lipid membranes on a tunable polymer cushion. *Phys. Rev. Lett.* **102,** 228102 (2009).
19. Wong, J. Y. *et al.* Polymer-cushioned bilayers. I. A structural study of various preparation methods using neutron reflectometry. *Biophys. J.* **77,** 1445–1457 (1999).
20. Sackmann, E. & Tanaka, M. Supported membranes on soft polymer cushions: Fabrication, characterization and applications. *Trends Biotechnol.* **18,** 58–64 (2000).
21. Watkins, E. B. *et al.* Structure and thermodynamics of lipid bilayers on polyethylene glycol cushions: Fact and fiction of PEG cushioned membranes. *Langmuir* **27,** 13618–13628 (2011).
22. Wagner, M. L. & Tamm, L. K. Tethered polymer-supported planar lipid bilayers for reconstitution of integral membrane proteins: Silane-polyethyleneglycol-lipid as a cushion and covalent linker. *Biophys. J.* **79,** 1400–1414 (2000).
23. Kraft, M. L., Weber, P. K., Longo, M. L., Hutcheon, I. D. & Boxer, S. G. Phase separation of lipid membranes analyzed with high-resolution secondary ion mass spectrometry. *Science* **313,** 1948–1951 (2006).
24. Yoon, T-Y. *et al.* Topographic control of lipid-raft reconstitution in model membranes. *Nature Mater.* **5,** 281–285 (2006).
25. Kahya, N., Scherfeld, D., Bacia, K., Poolman, B. & Schwille, P. Probing lipid mobility of raft-exhibiting model membranes by fluorescence correlation spectroscopy. *J. Biol. Chem.* **278,** 28109–28115 (2003).
26. Kaizuka, Y. & Groves, J. T. Structure and dynamics of supported intermembrane junctions. *Biophys. J.* **86,** 905–912 (2004).
27. Subramaniam, A. B., Lecuyer, S., Ramamurthi, K. S., Losick, R. & Stone, H. A. Particle/fluid interface replication as a means of producing topographically patterned polydimethylsiloxane surfaces for deposition of lipid bilayers. *Adv. Mater.* **22,** 2142–2147 (2010).
28. Dietrich, C. *et al.* Lipid rafts reconstituted in model membranes. *Biophys. J.* **80,** 1417–1428 (2001).
29. Pike, L. J. Rafts defined: A report on the Keystone symposium on lipid rafts and cell function. *J. Lipid Res.* **47,** 1597–1598 (2006).
30. Young, M. E. *et al.* The Sur7p family defines novel cortical domains in *Saccharomyces cerevisiae*, affects sphingolipid metabolism, and is involved in sporulation. *Mol. Cell. Biol.* **22,** 927–934 (2002).
31. Malinsky, J., Opekarová, M. & Tanner, W. The lateral compartmentation of the yeast plasma membrane. *Yeast* **27,** 473–478 (2010).
32. Smith, A. M., Vinchurkar, M., Gronbech-Jensen, N. & Parikh, A. N. Order at the edge of the bilayer: Membrane remodeling at the edge of a planar supported bilayer is accompanied by a localized phase change. *J. Am. Chem. Soc.* **132,** 9320–9327 (2010).

Acknowledgements

We thank the Harvard MRSEC (DMR-0820484), Harvard Center for Brain Science Imaging Facility, the Harvard Center for Nanoscale Systems, and Princeton University for partial support of this research. We also thank S. Lecuyer and M. Staykova for comments on the manuscript.

Author contributions

A.B.S. made the initial observation of the effects of glycans on supported lipid membranes. H.A.S. and A.B.S. initiated research. A.B.S. designed and performed experiments and analysed data. A.B.S., G.G., V.N.M. and H.A.S. interpreted data and wrote the paper.

Additional information

Supplementary information is available in the online version of the paper. Reprints and permissions information is available online at www.nature.com/reprints. Correspondence and requests for materials should be addressed to A.B.S. or H.A.S.

Competing financial interests

The authors declare no competing financial interests.